# Electron and phonon scattering in the high-temperature thermoelectric $La_3Te_{4-z}M_z$ ($M$=Sb,Bi)

Andrew F. May,[1,*] Espen Flage-Larsen,[2] and G. Jeffrey Snyder[3]
[1]*Chemical Engineering, California Institute of Technology, 1200 East California Blvd., Pasadena, California 91125, USA*
[2]*Department of Physics, University of Oslo, P.O. Box 1048, Blindern, NO-0316 Oslo, Norway*
[3]*Materials Science, California Institute of Technology, 1200 East California Blvd., Pasadena, California 91125, USA*
(Received 28 September 2009; revised manuscript received 2 February 2010; published 17 March 2010)

In this work, scattering mechanisms in the highly efficient thermoelectric material $La_{3-x}Te_4$ are investigated by controlling the carrier concentration via anion substitution in the nominally vacancy-free compositions $La_3Te_{4-z}Sb_z$ and $La_3Te_{4-z}Bi_z$. Through a comparison of the lattice thermal conductivity $\kappa_L$ in samples with and without Sb/Bi, this work reveals that La vacancies scatter phonons very efficiently and provide a ~100% reduction in $\kappa_L$ at 575 K. The addition of Sb or Bi leads to a significant reduction in the band gap, which is observed in the temperature-dependent transport data as well as first-principles calculations. Despite this significant change to the band structure, the transport parameters of the conduction band are only slightly modified. Also, an increase in the Hall mobility is observed at high $T$ and $z$, which is caused by a reduction in either the La-vacancy concentration or the electron's effective mass. A slight increase in thermoelectric efficiency is observed for nominal $La_3Te_{3.35}Sb_{0.65}$ at high $T$. Thus, the net result is a system with large thermoelectric efficiency and a tunable band gap, thereby enabling a clear example to examine the effect of band gap on thermoelectric properties.

DOI: 10.1103/PhysRevB.81.125205 PACS number(s): 72.15.Jf, 72.10.−d, 72.15.Eb, 72.20.Ee

## I. INTRODUCTION

Lanthanum telluride $La_{3-x}Te_4$ is an $n$-type conductor with high thermoelectric-conversion efficiency at temperatures above 1000 K. The compositions of interest, $0 \leq x \leq \frac{1}{3}$, possess the cubic $Th_3P_4$ structure type (space group $I\bar{4}3d$). In one formula unit of $La_3Te_4$, the La cations donate nine electrons and eight of these are required to satisfy the valence of the tellurium anions. There is thus one free electron per formula unit in $La_3Te_4$ (full La occupation, $x=0$) and the maximum carrier density of $n_{max} \sim 4.5 \times 10^{21}$ cm$^{-3}$ is achieved. La vacancies remove electrons from the system, and a metal-insulator transition exists; at $x=\frac{1}{3}$ the system is valance balanced with a band gap $E_g \sim 1$ eV.[1] The inherent carrier-density control and atomic disorder make this compound of interest for thermoelectric application, and the Jet Propulsion Laboratory sponsored investigations during the late 1980s.[2,3] Synthesis issues related to the La-Te phase diagram and sensitivity to oxidation, as well as the absence of an efficient $p$-type material, limited the advancement of $La_{3-x}Te_4$ at that time. New interest has been sparked by a low temperature, mechanical alloying synthesis that provides reproducible control of composition and optimization of thermoelectric performance,[4] as well as the discovery of $Yb_{14}MnSb_{11}$ as a complementary $p$-type material.[5]

An accurate description of the solid-state physics governing transport is generally required to improve a material's thermoelectric efficiency, which is governed by the figure of merit, $zT=\alpha^2 T/\rho\kappa$. Here, $\alpha$ is the Seebeck coefficient, $\rho$ the electrical resistivity, and $\kappa$ is the thermal conductivity. The coupling of $\alpha$, $\rho$, and the electronic component of the thermal conductivity ($\kappa_e$) makes obtaining large $zT$ difficult.[6] Additionally, even when a desired combination of the electronic properties is obtained, the lattice thermal conductivity ($\kappa_L$) must be small enough to permit large $zT$.

The coupling of lanthanum vacancies and carrier concentration makes it difficult to isolate the physics governing the thermoelectric phenomena in $La_{3-x}Te_4$. For instance, the impact of lanthanum vacancies on carrier mobility ($\mu$) is unclear. Vacancies are expected to influence carrier transport through scattering effects as well as a manipulation of the electronic structure. While the high-temperature mobility in heavily doped samples ($x<0.3$) appears to be limited by acoustic phonon scattering, the influence of multiple-scattering mechanisms is extremely difficult to isolate. Evidence for acoustic phonon scattering is found in the dependence of the Hall mobility ($\mu_H$) on temperature and Hall carrier concentration ($n_H$).[2,4] The electronic structure further complicates the relationship between vacancy concentration and mobility, as a light band exists at the minimum conduction energy (the band probed when $x$ is large) and heavy bands contribute significantly to transport when $x$ is small.[1] The inherent mobility of the light band is expected to be larger than that of the heavy bands (found at higher energy), and thus it may conceal the scattering effects associated with La vacancies. Also, a transition from itinerant to hopping conduction (due to Anderson localization) is expected as the vacancy count approaches the maximum value of $x=\frac{1}{3}$.[7]

The impact of lanthanum vacancies on thermal transport is intuitive—the point defects scatter phonons. Their influence is easily observed at high $x$ values, where a low, nearly temperature-independent lattice thermal conductivity is observed ($\kappa_L \sim 0.6$ W/m/K at 500 K). This is expected because the randomly distributed vacancies are present in very high concentrations (up to $\frac{1}{9}$ La vacant), and vacancies are essentially the ideal point defect for phonon scattering because they provide the maximum mass contrast. Our prior work suggested that, at very low $x$, the value of $\kappa_L$ is again ~0.5 W/m/K at moderate $T$. This was believed to be evidence for electron-phonon coupling at high temperature. The nominal compositions $La_3Te_{4-z}Sb_z$ were selected to investigate the possible role of electron-phonon scattering because the mass contrast between Sb and Te is small, which mini-

 

mizes the point-defect scattering associated with carrier-concentration control. The current study also benefits from recent heat-capacity measurements on $La_3Te_4$ (Ref. 9), which suggest a larger $C_P$ than previously utilized is required; this results in $\kappa_L \sim 1$ W/m/K for $La_3Te_4$ near 500 K.

To further investigate the physics governing transport in $La_{3-x}Te_4$, samples of nominal composition $La_3Te_{4-z}Sb_z$ and $La_3Te_{4-z}Bi_z$ were prepared, and the thermal transport properties of pure $La_{3-x}Te_4$ were recalculated in light of new $C_P$ data. The anionic substitutions of $Sb^{3-}$ and $Bi^{3-}$ for $Te^{2-}$ reduce the free-electron concentration because an additional electron is required to complete anion valence (relative to Te). In ideal $La_3Te_{4-z}Sb_z$ and $La_3Te_{4-z}Bi_z$ compounds, the carrier density can be estimated by $n=n_{max}(1-z)$, whereas in pure $La_{3-x}Te_4$ the relationship is $n=n_{max}(1-3x)$. Therefore, these anionic substitutions theoretically allow carrier concentration control in the absence of vacancies and thus facilitate the investigation of phonon- and electron-scattering mechanisms.

This article considers the scattering of phonons via electrons and vacancies, as well as the impact of the anionic substitution on the electronic structure and transport. To aid in the investigation, density-functional theory (DFT) was utilized to calculate the electronic structures of $La_3Te_4$, $La_3Te_3Sb$, and $La_3Te_3Bi$. While these ideal structures cannot account for the disorder inherent to these systems, they provide approximations which are valid starting points for understanding the influence of these elemental substitutions, much like the prior calculations on $La_3Te_4$.[1]

## II. METHODS

### A. Synthesis

Samples were prepared in a manner similar to the $La_{3-x}Te_4$ samples with which they are compared.[4] Synthesis occurred via high-energy ball milling, where a SPEX 8000 series Mixer/Mill was employed. In an argon dry box, the raw elements are combined with stainless steel balls in stainless steel vial, and milling was completed in less than a day. The fine powders were consolidated at temperatures greater than 1300 K while roughly one metric ton of force was applied over a 1.2 cm diameter. An alcohol-based lubricant was utilized when cutting the samples to 1 or 2 mm disks for measurement, or when polishing samples for microscopy, as they are sensitive to aqueous solutions.

### B. Characterization

Phase purity was determined with x-ray diffraction, which was performed on a Phillips X'Pert Plus diffractometer (Cu source, current of 40 mA, and a voltage of 45 kV), and via electron probe microanalysis (EPMA) performed on a JEOL JXA-8200. Chemical composition was obtained during EPMA using wavelength dispersive spectroscopy (WDS), which analyses roughly a cubic micron per point using a voltage of 15 kV. During WDS, elemental Te, Sb, Bi, and $LaPO_4$ were utilized as standards for Te, Sb, Bi, and La, respectively, and a ZAF correction is employed to account for atomic number ($Z$), absorption, and fluorescence effects.

Electrical transport was probed via Hall coefficient ($R_H$), electrical resistivity ($\rho$), and Seebeck coefficient ($\alpha$) measurements. The van der Pauw method was employed for Hall effect and electrical resistivity measurements. During high-temperature Hall effect measurements a magnetic field of $\sim 1$ T was utilized, and room-temperature Hall data were collected on a different instrument using $\sim 2$ T. Seebeck coefficients were obtained using the differential light pipe method discussed by Wood with W/Nb thermocouples.[8] Thermal conductivity was obtained via $\kappa=D_T C_P d$, where $d$ is the density and the thermal diffusivity $D_T$ was obtained from a NETZSCH LFA 457. Heat-capacity $C_P$ data were taken from Ref. 9 and were obtained via differential scanning calorimetry on a sample of nominal composition $La_3Te_4$.[9] We note this $C_P$ differs from that in a previous publication.[4] At high temperatures, the change in $C_P$ due to compositional variation is mostly determined by a change in the electronic contribution (the change due to average atomic mass is very small for Sb substitution, though for Bi substitution these effects are nearly equal). For the samples with lowest $n$ (highest $x$ or $z$), the $C_P$ is likely overestimated by about $\sim 6\%$ at 1200 K because the $C_P$ with the highest electronic contribution is utilized for all samples. All transport measurements were performed under dynamic vacuum. The majority of these measurements were performed at the Jet Propulsion Laboratory, while some data were collected at Caltech.

### C. Density-functional calculations

The electronic structures of $La_3Te_4$, $La_3Te_3Sb$, and $La_3Te_3Bi$ were calculated within the density-functional theory framework of the Vienna *ab initio* simulation package.[10,11] Even though these valence-balanced ternary compounds have never been synthesized and are likely to contain significant anion-site disorder, these calculations serve as an approximate model to shed light on the role of the substitution of Sb or Bi for Te. The calculations employed the Perdew-Burke-Ernzerhof[12] exchange-correlation functional in the generalized gradient approximation. In the absence of experimental lattice parameters for $La_3Te_3Sb$ and $La_3Te_3Bi$, relaxations of the structures were performed using the experimental lattice parameter[13] of $La_3Te_4$ as input. Four out of 16 Te atoms were exchanged for Sb or Bi within the original unit cell to obtain the $La_3Te_3Sb$ and $La_3Te_3Bi$ stoichiometries, respectively. The structures were relaxed in both cell shape, volume, and atomic positions using a residual minimization, direct inversion in the iterative subspace scheme.[14] For comparison reasons, the relaxed $La_3Te_4$ structure was utilized.

An energy cutoff of 650 eV and a $\Gamma$-centered $k$-point sampling of $9\times9\times9$ were sufficient to converge the electronic structures. The density of states was obtained from a second run using the modified linear tetrahedron method.[15]

The Te positions in the relaxed $La_3Te_4$ differs by 5–8 % (see Table I for the diagonal lattice constants and Wyckoff positions) of the experimental structure reported in Ref. 13, while the change in the La positions are within 1%. Slight

TABLE I. Experimental lattice parameter of $La_3Te_4$, Ref. 13, and computational lattice parameters for the relaxed $La_3Te_4$, $La_3Te_3Sb$, and $La_3Te_3Bi$ cells. Wyckoff positions of $La_3Te_3Sb$ and $La_3Te_3Bi$ are strictly not valid (symmetry breaking), but are given for comparison reasons.

| | Unit cell (Å) | | | | Wyckoff position | | |
|---|---|---|---|---|---|---|---|
| | *a* | *b* | *c* | | *x* | *y* | *z* |
| $La_3Te_4$ (exp) | 9.634 | 9.634 | 9.634 | La | 0.375 | 0.000 | 0.250 |
| | | | | Te | 0.083 | 0.083 | 0.083 |
| $La_3Te_4$ | 9.687 | 9.687 | 9.687 | La | 0.375 | 0.000 | 0.250 |
| | | | | Te | 0.076 | 0.076 | 0.076 |
| $La_3Te_3Sb$ | 9.692 | 9.686 | 9.690 | La | 0.375 | 0.000 | 0.250 |
| | | | | Te | 0.075 | 0.076 | 0.076 |
| | | | | Sb | 0.080 | 0.081 | 0.081 |
| $La_3Te_3Bi$ | 9.741 | 9.736 | 9.742 | La | 0.375 | 0.000 | 0.251 |
| | | | | Te | 0.074 | 0.075 | 0.075 |
| | | | | Bi | 0.079 | 0.080 | 0.080 |

distortions of the symmetry of the unit cell of $La_3Te_3Sb$ and $La_3Te_3Bi$ were observed, and were found to be less than 1% (based on the full lattice constant matrix). Hence, only the diagonal of the relaxed lattice vectors are given in Table I. The Sb and Bi sites change by approximately 1% with respect to the relaxed Te sites of $La_3Te_4$. The discrepancy between the relaxed and experimental lattice parameters of $La_3Te_4$ stem from a DFT failure of properly describing the heavy elements and is most likely related to the well-known delocalization error. Due to the localization of the La *f* and Te *d* states, this error is particularly important in these systems. Relaxations of the Sb- and Bi-filled structures are within 1% of the relaxed $La_3Te_4$ structure and due to later comparisons we persist on using the relaxed $La_3Te_4$ parameters throughout this work. Comparisons of the band structure near the Fermi level reveal no significant change except a small shift of the La *f* states in the conduction band to lower energies in the relaxed $La_3Te_4$ structure. In addition, the band gap remains approximately constant upon relaxation. A unit-cell expansion is observed upon the substitution of Sb or Bi for Te, which is expected due to size differences.

The electronic structure obtained for $La_3Te_4$ is consistent with that in Ref. 1, where a slightly smaller band gap (0.95 eV) was obtained due to the inclusion of spin-orbit coupling. The main effects of spin-orbit coupling in $La_3Te_4$ appear to be a small reduction in band gap and a 0.03 eV splitting of degenerate bands near the Fermi level (for the energies of interest).

## III. RESULTS AND DISCUSSION

Samples were found to be phase pure by x-ray diffraction and electron-probe microanalysis. The diffraction scan in Fig. 1 is for the sample that contains the highest nominal antimony content ($La_3Te_{3.2}Sb_{0.8}$, sample Sb5), and all peaks can be assigned to the desired crystal structure. High density (>94% theoretical) was observed for all Sb and Bi containing samples. Compositional data are shown in the inset of Fig. 1, where experimental Sb and Bi content (at.%) are plotted versus nominal content and the amount of Sb (Bi) found in the samples is consistent with the nominal composition.

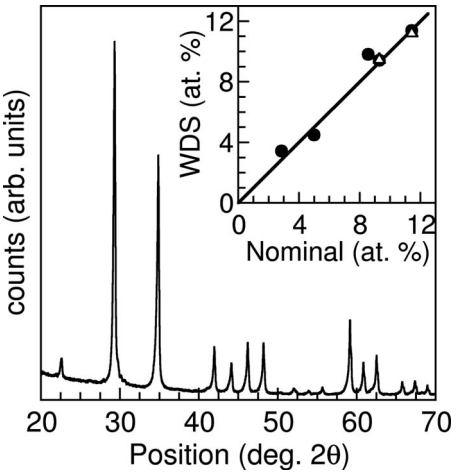


FIG. 1. X-ray diffraction scan of sample with nominal composition $La_3Te_{3.2}Sb_{0.8}$ shows no impurity phase, which is representative of the samples in this study. The inset shows compositional data obtained via WDS plotted versus nominal composition; the atomic percentage of Sb (filled circles) and Bi (open triangles) agree well with the desired content (solid line).

### A. Electrical transport

As shown in Table II, the magnitudes of the Seebeck coefficients and electrical resistivity increase with increasing Sb or Bi content, and the Hall carrier density $n_H=1/R_He$ decreases with increasing Sb content. This is expected for the substitution of $^-3$ anion (Sb, Bi) for a $^-2$ anion (Te) in an *n*-type semiconductor. The expected relationship between carrier-density and nominal composition is also observed in pure $La_{3-x}Te_4$ samples, where the introduction of La vacancies reduces the carrier concentration.[4]

TABLE II. Nominal composition along with Hall density ($=1/R_H$) and electrical resistivity at 300 K and Seebeck coefficient at 400 K. Data for $La_{3-x}Te_4$ is taken from Ref. 4.

| Sample ID | Nominal composition | $n_H$ ($10^{21}$ cm$^{-3}$) | $\rho$ (mΩ cm) | $\alpha$ ($\mu$V/K) |
|---|---|---|---|---|
| Sb1 | $La_3Te_{3.80}Sb_{0.20}$ | 2.9 | 0.53 | −45 |
| Sb2 | $La_3Te_{3.65}Sb_{0.35}$ | 1.3 | 1.1 | −53 |
| Sb3 | $La_3Te_{3.40}Sb_{0.60}$ | 0.54 | 9.0 | −74 |
| Sb4 | $La_3Te_{3.35}Sb_{0.65}$ | 0.35 | 18 | −91 |
| Sb5 | $La_3Te_{3.20}Sb_{0.80}$ | 0.08 | 43 | −148 |
| Bi1 | $La_3Te_{3.35}Bi_{0.65}$ | 0.39 | 7.1 | −71 |
| Bi2 | $La_3Te_{3.20}Bi_{0.80}$ | 0.39 | 10 | −76 |
| LT1 | $La_{2.99}Te_4$ | 4.1 | 0.61 | −41 |
| LT2 | $La_{2.74}Te_4$ | 0.52 | 2.7 | −88 |
| LT3 | $La_{2.72}Te_4$ | 0.12 | 8.8 | −175 |

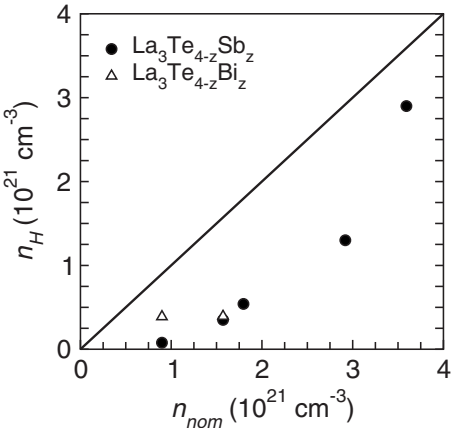


FIG. 2. The experimental Hall carrier density $n_H = 1/R_H e$ at room temperature versus the theoretical carrier density obtained from charge counting for nominal $La_3Te_{4-z}Sb_z$ and $La_3Te_{4-z}Bi_z$. The experimental carrier density is always less than the expected value (solid line) and the discrepancy is likely due to the presence of La vacancies.

As shown in Fig. 2, the experimental values of $n_H$ are consistently lower than those expected from valence counting assuming nominal composition, and the relative deviation is greatest at large Sb (Bi) content. The primary source for reduced $n_H$ is likely to be the presence of lanthanum vacancies, which remove electrons from the system and thus reduce $n_H$. Vacancy formation may be promoted by the presence of Sb or Bi in the crystal. However, simple valence counting would suggest that the sample with the most Sb is not the sample with the largest vacancy concentration, and thus the driving force for vacancy formation does not seem to be proportional to Sb or Bi content. It is possible that the presence of Sb or Bi modifies the mechanical alloying synthesis and promotes the loss of one species (or some binary compound) over another. In general, the mechanical alloying synthesis may have a systematic loss of one species over another due to differences in brittleness or ductility (elements may preferentially stick to vial) or reactivity. The vacancy count in $La_{3-x}Te_4$ can reach $x=\frac{1}{3}$, and $x \sim 0.12$ is the maximum $x$ required to satisfy the electron count in the Sb or Bi systems (found in Sb2), and thus the $x$ values needed to explain these trends are quite reasonable. Note that cationic Sb substitution for La does not provide an explanation for the observed trend in carrier concentration. Vacancy formation may be promoted by the formation of $La_4Sb_3$ (anti-$Th_3P_4$ structure type), though identifying this phase is extremely difficult due to the similar lattice parameters and atomic masses. One interesting possibility is anionic (acceptor) Sb sitting on a La site in $La_{3-x}Te_4$, which would reduce the carrier concentration and could certainly manipulate electronic transport.

Scattering mechanisms can also produce a variation between $n_H$ and the chemical $n$, which is the $n$ associated with charge counting. The influence of scattering effects are manifested in the Hall factor, $r_H = n/n_H$. As will be shown below, large Sb (Bi) addition modifies electron conduction, and thus likely leads to a change in $r_H$ relative to the pure $La_{3-x}Te_4$ samples (or samples with low Sb content). The influence of

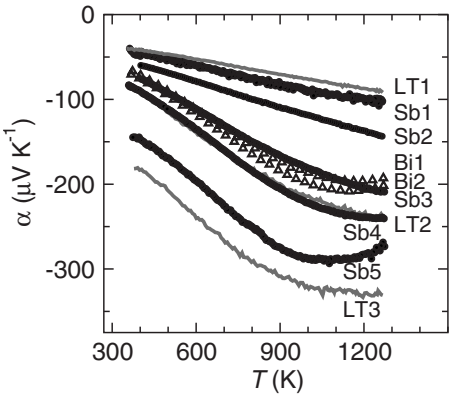


FIG. 3. Temperature dependence of Seebeck coefficients for $La_3Te_{4-z}Sb_z$ (closed circles) and $La_3Te_{4-z}Bi_z$ (open triangles) are similar to those of the pure $La_{3-x}Te_4$ samples (Ref. 4) (solid gray curves). The maximum value of $|\alpha|$ and the corresponding temperature suggest that the band gap is reduced by Sb addition, and is further reduced by Bi addition.

$r_H$ is relatively small compared to stoichiometry, as $r_H = 1.93$ and 1.18 are the upper limits of $r_H$ when the carrier mobility is limited by ionized impurity scattering and acoustic phonon scattering, respectively.[16]

The temperature dependence of the Seebeck coefficients is shown in Fig. 3. The magnitude and temperature dependence of $\alpha$ in the Sb containing (filled circles) and Bi containing samples (open triangles, every other data point removed for clarity) are similar to that of pure $La_{3-x}Te_4$ samples (gray curves). At high temperature, where acoustic phonon scattering should limit the carrier relaxation time regardless of sample composition, the dependence of the Seebeck coefficient on carrier density is found to be similar for all samples. This is shown in Fig. 4, where the magnitude of $\alpha$ at 1000 K is plotted versus the room temperature $n_H$. The minor changes in $\alpha$ imply that the conduction band does not change significantly upon Sb or Bi substitution for Te, which is consistent with the DFT results presented below. However, it is possible the effective mass is lower in the Sb- or Bi-

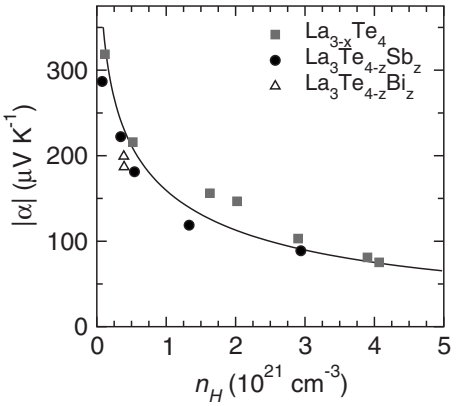


FIG. 4. The dependence of Seebeck coefficient at 1000 K on the room-temperature Hall carrier concentration is similar for $La_3Te_{4-z}Sb_z$, $La_3Te_{4-z}Bi_z$, and pure $La_{3-x}Te_4$ samples, Ref. 4, implying little change to the conduction band occurs upon substitution. Also shown is a single parabolic band model (solid curve).

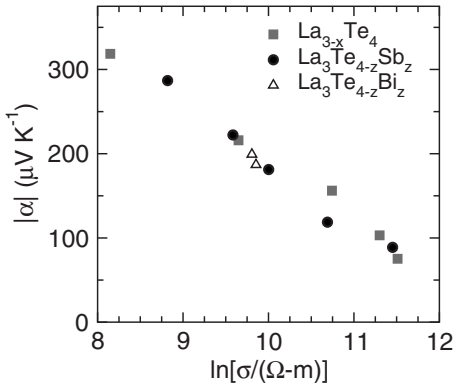


FIG. 5. Seebeck coefficient as a function of the natural logarithm of the electrical conductivity (at 1000 K) demonstrates similarity of electrical transport in all samples at high $T$, where it is assumed acoustic phonon scattering limits the carrier mobility.

substituted compounds, as suggested by the slight suppression of the Seebeck coefficient at low $n_H$. Less variation in the electronic properties of these samples is observed when $|\alpha|$ is plotted as a function of $\ln(\sigma)$ at 1000 K, see Fig. 5. This implies any reduction in $|\alpha|$ (for a given $n$) associated with band mass is compensated for by an increase in $\mu$. Such a trend is consistent with the relationship between mobility and effective mass, $\mu \propto 1/m^*$; scattering effects can cause an even stronger variation in $\mu$ as $m^*$ changes. The apparent increase in $|\alpha|$ for pure $La_{3-x}Te_4$ samples near $2 \times 10^{21}$ cm$^{-3}$ is likely related to the electronic structure (heavy bands are found at ~0.3 eV above the low-mass, minimum-energy bands),[1] although experimental error must also be acknowledged.

The single parabolic band model shown in Fig. 4 (solid curve) is generated utilizing[16]

$$\alpha = \frac{k}{e}\left(\frac{\int_0^\infty \epsilon^{5/2}\tau\frac{\partial f}{\partial \epsilon}d\epsilon}{\int_0^\infty \epsilon^{3/2}\tau\frac{\partial f}{\partial \epsilon}d\epsilon} - \eta\right) \quad (1)$$

and

$$n = 4\pi\left(\frac{2m^*kT}{h^2}\right)^{3/2} F_{1/2}(\eta), \quad (2)$$

where

$$F_r(\eta) = \int_0^\infty \epsilon^r f(\eta) d\epsilon. \quad (3)$$

Here, $\epsilon$ and $\eta$ are the reduced carrier energy and reduced electrochemical potential, respectively, $f$ is the Fermi distribution, and $\tau$ and $m^*$ are the carrier relaxation time and effective mass, respectively. The chemical $n$ is employed in Fig. 4 because the scattering effects that are present at room temperature (where the $n_H$ data were collected) are not isolated for large Sb (Bi) content. If the effect of $r_H$ were included and a theoretical $|\alpha|$ versus $n_H$ was plotted, the curve would shift to lower $n_H$ values, particularly for the low $n_H$ samples. The parabolic band model in Fig. 4 is generated utilizing a theoretical description for $\tau$ limited by acoustic phonon scattering,[16]

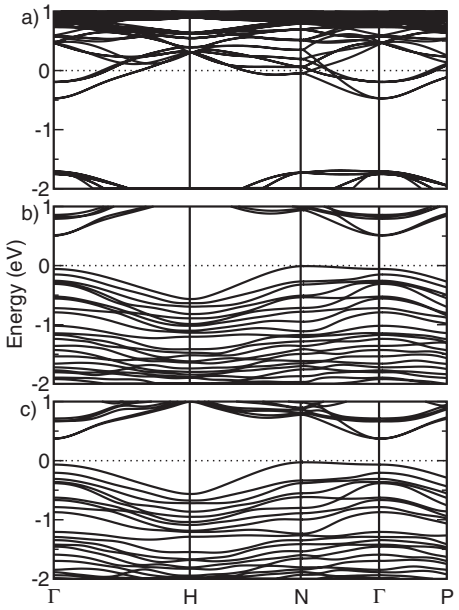


FIG. 6. The calculated electronic structures of (a) $La_3Te_4$, (b) $La_3Te_3Sb$, and (c) $La_3Te_3Bi$ shown for the relevant energy range.

$$\tau_L = \frac{\pi\hbar^4 v_l^2 d}{\sqrt{2}E_{def}^2 (m^*kT)^{3/2}\epsilon^{1/2}}, \quad (4)$$

where $E_{def}$ is the deformation potential, $v_l$ the longitudinal speed of sound, and the subscript $L$ stands for lattice scattering. Here, the fundamental constants and material parameters are removed from the integration and cancel, thus only the energy dependence remains. An effective mass of $m^* = 2.8m_e$ was utilized to calculated $n$ via Eq. (2).

The primary effect of Sb or Bi substitution on $\alpha$ is a compensation of $\alpha$ at high $T$ and large $z$, which is caused by the thermal excitation of minority carriers. This is evidence for a reduced band gap in samples with high Sb or Bi content, as $La_{3-x}Te_4$ samples showed this feature at lower $n$ and higher $T$. The thermal gap can be estimated by the maximum in $|\alpha|$ versus $T$, $E_g = 2e\alpha_{max}T_{max}$,[17] which yields $E_g \sim 0.46$ eV for the two Bi containing samples, $E_g \sim 0.63$ eV for sample Sb5, and $E_g \sim 0.83$ eV was obtained for $La_{3-x}Te_4$.[4] A reduced energy gap is also inferred, in a similar manner, from the $\rho$ and $\kappa$ data below.

The experimental observation of reduced energy gap upon Sb or Bi substitution is consistent with the DFT calculations. The DFT calculations on the idealized $La_3Te_4$, $La_3Te_3Sb$, and $La_3Te_3Bi$ compounds suggest the primary effect of Sb or Bi substitution is to raise the energy of the valence band, where the majority of Te, Sb, and Bi states are located, and thus the substitutions result in a reduction in the energy gap (see Fig. 6). The most noticeable change to the conduction band with Sb (Bi) substitution is the splitting of heavy, degenerate bands at the Γ point near 0.3 eV above the minimum conduction energy. The substitutions also flatten these bands somewhat, and thus an increased band mass may be

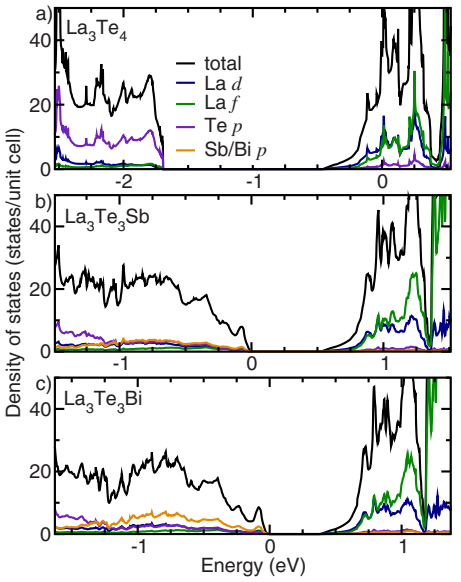


FIG. 7. (Color online) The projected DOS reveals a decreasing energy gap for (a) $La_3Te_4$, (b) $La_3Te_3Sb$, and (c) $La_3Te_3Bi$. A total of 3 eV is shown for all panels.

expected at high-doping levels. However, the changes in electronic structure are predicted for high Sb or Bi concentration, and it is thus not surprising that the samples with low Sb content and high $n_H$ do not show an increased band mass. Therefore, a dramatic change in the Seebeck coefficient ($n$ type) is not expected with these anionic substitutions (at moderate $T$), which is in agreement with the experimental data. These results imply cation substitutions are required to significantly modify the conduction bands in $La_{3-x}Te_4$ (primarily composed of La states) and provide large changes in the Seebeck coefficient.

The DFT energy gaps are most easily observed in the density of states (Fig. 7), where $E_g$ of 1.22, 0.51, and 0.38 eV are calculated for $La_3Te_4$, $La_3Te_3Sb$, and $La_3Te_3Bi$, respectively. To further validate these trends, the band structure of isostructural $La_3S_4$ was calculated and an energy gap of 2.07 eV was observed; the larger gap of $La_3S_4$ is consistent with prior calculations[18] and the increasing electronegativity as one moves from Te to S. Note the Fermi level (0 eV) is placed within the conduction band for $La_3Te_4$ because it has one free electron per formula unit, and the Fermi level for $La_3Te_3Sb$ and $La_3Te_3Bi$ is at the top of the valence band because these are valence-balanced compositions.

In Fig. 8(a), the electrical resistivity of Sb containing compounds (filled circles) are compared to that of sample LT3 (gray curve), which has the highest resistivity of the heavily doped $La_{3-x}Te_4$ samples. In Fig. 8(b), the less resistive samples are examined in further detail, along with samples containing Bi (open triangles) and the two less resistive $La_{3-x}Te_4$ samples (gray curves). At low Sb content (and low Bi content, not shown), electrical conduction is very similar to that in $La_{3-x}Te_4$, which makes physical sense because these samples have high carrier concentrations and similar composition. The linear increase in $\rho$ with increasing $T$ implies acoustic phonon scattering limits the carrier mobility, which is consistent with the data for $La_{3-x}Te_4$ (even for large $x$).

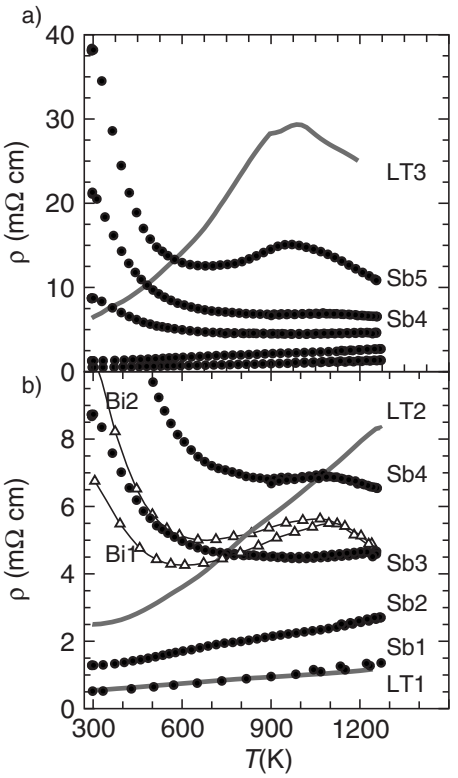


FIG. 8. The resistivity of $La_3Te_{4-z}Sb_z$ at low Sb content is similar to that of pure $La_{3-x}Te_4$ samples, and as Sb content increases an activated process emerges. Panel (b) also includes $La_3Te_{4-z}Bi_z$ samples, which display similar behavior.

The expected heavily doped behavior (positive $d\rho/dT$ at moderate $T$) is lost at large Sb or Bi content, and activated conduction is observed at moderate $T$ for $z \geq 0.6$. This is shown in Fig. 8, where resistivity decreases with increasing $T$ for large $z$ and moderate $T$. The source for activated conduction is unknown; it could be caused by the substitution of Sb for Te which promotes local variations in the electric potential associated with the randomly distributed anions, or defects or impurities which may be promoted by large Sb (Bi) concentrations. The decrease in $\rho$ with increasing $T$ is primarily associated with a change in the carrier mobility, not carrier density, as demonstrated by the temperature dependences of $n_H$ and $\mu_H$ in Figs. 9(a) and 9(b), respectively.

Above ~550 K, the mobility in the Sb containing sample (Sb5) is larger than the mobility in the $La_{3-x}Te_4$ (LT3) sample. The larger mobility in Sb5 at high $T$ may be related to the reduction in La vacancies, which are likely scattering sources in $La_{3-x}Te_4$ when $x$ is large. The Seebeck coefficient data in Fig. 4 imply a minor reduction in effective mass, which would also promote an increased mobility [consider Eq. (4) and the classic definition $\mu = e\tau/m$].

Activated conduction is inferred from the $\mu_H(T)$ shown in Fig. 9(b). However, due to the small temperature range over which the activated behavior is observed in this high-temperature study, a variety of models are found to adequately fit the data. In particular, small polaron and variable range hopping (three dimensional) both provide a reasonable description of the data in Fig. 9(b). For the sake of simplicity, we report a generic activation energy ($\mu_H \propto \exp[E_a/kT]$) for

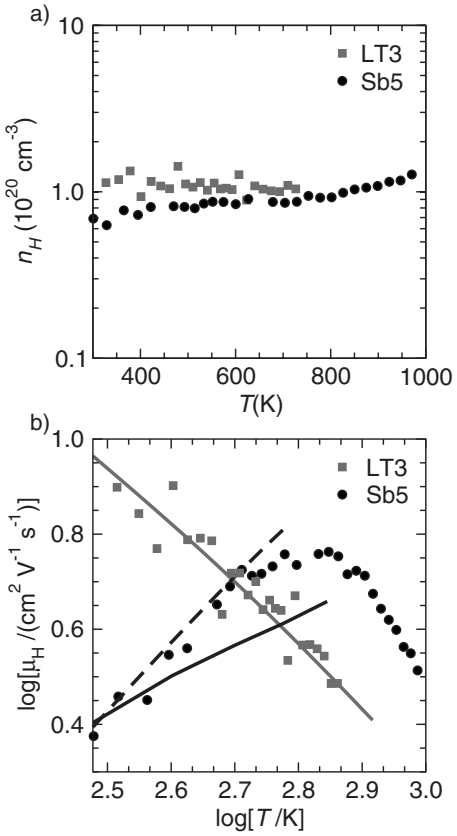


FIG. 9. Temperature dependence of (a) Hall carrier concentration and (b) the Hall mobility for the samples containing the most Sb (solid markers) and highest vacancy content (LT3). The Hall mobility of the $La_{3-x}Te_4$ sample (gray markers) decays with increasing temperature as expected for simple acoustic phonon scattering, the theoretical description of which is shown by the solid gray curve. The mobility of the nominal $La_3Te_{3.2}Sb_{0.8}$ sample (Sb5) increases with increasing $T$ for moderate $T$, and decreases with increasing $T$ at high $T$. The rise in $\mu_H$ with $T$ may be associated with ionized impurity scattering, a theoretical temperature dependence for this is represented by the black curve; the dashed curve shows $T^{3/2}$ behavior.

the data in Fig. 9(b). In the range 300–600 K, an activation energy of $E_a$=0.06 eV is obtained.

Anderson localization is a type of activated conduction studied by Cutler and Mott in $Ce_{3-x}S_4$,[7] which is another rare-earth chalcogenide possessing the $Th_3P_4$ structure type. In their study, Cutler and Mott concluded that the random distribution of Ce vacancies promotes Anderson localization.[7] However, in $Ce_{3-x}S_4$, localization was only observed at low temperatures and/or very low $n$ ($x \rightarrow \frac{1}{3}$). For instance, the most conductive $Ce_{3-x}S_4$ sample to display this behavior had a room-temperature resistivity of ~25 m$\Omega$ cm, and displayed predominantly itinerant conduction down to ~100 K where the onset of localization was observed. We did not observe localization in phase pure $La_{3-x}Te_4$ samples for the temperatures ($T$>300 K) and doping levels considered here;[4] low-temperature studies have yet to be performed. Activated $\rho(T)$ was observed near room temperature in two samples that were not phase pure, though this effect was not present past 400 K and was very minor in comparison to the observation in Sb- and Bi-doped samples in this study. The behavior in these impurity containing samples was not reproducible in phase pure $La_{3-x}Te_4$, whereas activated behavior was reproduced by multiple synthetic efforts and procedures (for instance, additional annealing time was considered) in the Sb and Bi containing samples. Recall the Sb- and Bi-doped samples are phase pure by the same characterization techniques that identified the impurities believed responsible for the observation of small deviations from itinerant conduction (assumed due to "dirty" grain boundaries) in $La_{3-x}Te_4$.

The temperature dependence of $\mu_H$ for sample Sb5 may be explained by the conventional theory of itinerant electron conduction with multiple-scattering sources. In this framework, the increase in $\mu_H$ with increasing $T$ at moderate $T$ is due to ionized impurity scattering (by Sb or Bi anions), and the decrease in $\mu_H$ at high $T$ is caused by acoustic phonon scattering. The general expression for $\mu_H$ in a single parabolic band is

$$\mu_H = R_H\sigma = \frac{e}{m^*}\frac{\int_0^\infty \epsilon^{3/2}\tau^2\frac{\partial f}{\partial \epsilon}d\epsilon}{\int_0^\infty \epsilon^{3/2}\tau\frac{\partial f}{\partial \epsilon}d\epsilon}. \quad (5)$$

This differs slightly from the description of the drift mobility due to scattering effects.[16] To utilize this equation and Eq. (1), the carrier relaxation time $\tau$ must be obtained via appropriate summation of all contributing scattering times, $\tau^{-1}=\Sigma_1^n\tau_j^{-1}$. $\tau_j$ can often be modeled by power-law energy dependence with an appropriate prefactor, $\tau_j=\tau_{0,j}\epsilon^{\lambda-1/2}$ and the value of $\lambda$ depends on the scattering mechanism. Difficulty utilizing Eq. (5) arises due to the dependence of $\mu_H$ on $\eta$ as well as the functional forms of the various $\tau_j$ (the prefactor $\tau_{0,j}$ is not always independent of energy). In general, the experimentalist obtains an approximate temperature-dependent $\eta$ from the temperature dependence of the Seebeck coefficient utilizing Eq. (1). The values of $\eta(T)$ are difficult to obtain when multiple-scattering mechanisms are present, and an additional measurement is generally required to allow a more complete solution to be obtained. In the limit of high or low $T$, a single-scattering mechanism may limit $\mu_H$, which allows $\eta(T)$ to be obtained more easily. Clearly, the reliability of such a treatment rests heavily on the electronic structure, which is assumed to be well described by a parabolic band. The samples analyzed here (LT3 and Sb5) have relatively low-doping levels and transport is likely to be determined by only the minimum-energy conduction band, which is, to first order, parabolic.

First consider the temperature dependence of $\mu_H$ for the $La_{3-x}Te_4$ sample (LT3) in Fig. 9(b). The decay of $\mu_H$ in LT3 with increasing $T$ is well described by the theory of acoustic phonon scattering, which is shown by the solid gray curve in Fig. 9(b). This curve is generated using Eqs. (1), (4), and (5) with $m^*=2.8m_e$ and $v_l$=3580 m/s based on the earlier work for $La_{3-x}Te_4$.[4] The only free parameter is the deformation potential, and a value of $E_{def}$=6.1 eV is obtained by fitting the data between 300 and 725 K for sample LT3. The value

of $E_{def}$ is in fair agreement with early work describing the $n_H$ dependence of $\mu_H$ in $La_{3-x}Te_4$, though a slightly different representation was utilized.[4] The temperature dependence of $\mu_H$ for sample LT3 in Fig. 9(b) differs from the $T^{-3/2}$ decay implied by Eq. (4) because the decrease in $\eta$ with increasing $T$ impacts $\mu_H$ via the integrals in Eq. (5). Temperature-dependent $m^*$, $v_l$, and $E_{def}$ can also effect the magnitude or temperature dependence of $\mu_H$ significantly. A change in one or all of these material properties with Sb substitution may explain the difference between the $\mu_H$ for samples Sb5 and LT3 at high $T$, where acoustic phonon scattering likely limits $\mu_H$ regardless of composition.

In the limit of only ionized impurity scattering, the carrier relaxation time can be described by[19]

$$\tau_i = \frac{16\sqrt{2m^*}\pi\chi^2(kT)^{3/2}\epsilon^{3/2}}{N_i Z^2 e^4 g}, \tag{6}$$

where $\chi$ is the permittivity, $Z$ the effective charge, $N_i$ is the concentration of impurity ions, and $g$ is given by

$$g = \ln(1+b) - \frac{b}{1+b}, \tag{7}$$

where

$$b = \frac{8m^*\epsilon kT}{\hbar^2}\frac{\chi kTF[0.5,\eta]}{ne^2F[-0.5,\eta]}. \tag{8}$$

For illustrative purposes, we compare the moderate $T$ behavior of $\mu_H$ for sample Sb5 with a theoretical curve (solid black line) generated from Eqs. (1) and (5)–(8). The theoretical curve is generated assuming the nominal composition for $N_i$, $m^*=2.8m_e$, and $\chi=27\epsilon_0$ is obtained by fitting to the room-temperature data ($\epsilon_0$ is the permittivity of free space). The deviation from this theoretical curve and the experimental data can be easily explained by temperature-dependent $m^*$ or $\chi$, though other sources of error include the single-band approximation, temperature-independent $n=8\times10^{19}$ cm$^{-3}$, and the inclusion of only one type of scattering. In this case, a temperature-dependent $m^*$ could result from the multiband features and the increased occupation of states associated with thermal broadening (recall this is a parameterized, single-band effective mass). The dashed black line in Fig. 9(b) demonstrates $T^{3/2}$ behavior commonly associated with ionized impurity scattering in the nondegenerate limit.

### B. Thermal transport

The thermal diffusivity and conductivity are shown as a function of temperature in Fig. 10. For moderate temperatures, all samples behave similarly and $D_T$ and $\kappa$ generally decrease with increasing $T$ and decreasing $n_H$. At high temperatures, $D_T$ and $\kappa$ rises in the samples containing Bi (open triangles) or large amounts of Sb. This is due to the thermal excitation of charge carriers across the energy gap, which occurs more readily in the samples with Sb and Bi due to the reduced energy gap.

In the absence of heat-capacity data for all compositions, the values of $C_P$ utilized were taken from Ref. 9 for $La_3Te_4$. The introduction of vacancies (loss of electronic heat capacity) resulted in less than a 3% change in $C_P$ at room temperature for $La_{3-x}Te_4$, which is relatively minor compared to the dependence of other transport properties (such as electrical conductivity) on composition. While some changes in $C_P$ with elemental substitution are expected due to changes in average atomic mass, these effects are estimated to be less than 7% for the Bi compounds (a decrease in $C_P$ is expected) and less than 1% for the Sb compounds (an increase in $C_P$ is expected) for complete substitution ($z=1$).

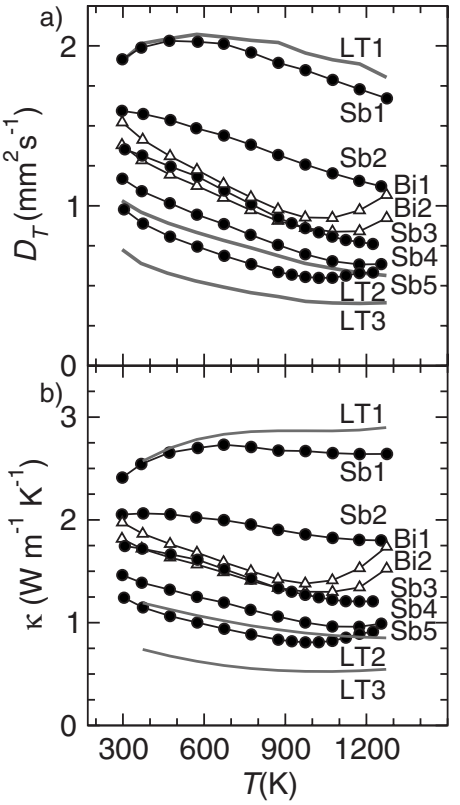


FIG. 10. (a) The thermal diffusivity and (b) thermal conductivity decreases with decreasing carrier concentration (increasing Sb content) and increasing temperature. The thermal activation of carriers increases $D_T$ and $\kappa$ at high temperature, and is observed in the Sb and Bi containing samples because these elemental substitutions lead to a reduced energy gap.

The lattice thermal conductivity ($\kappa_L$) was estimated by subtracting the electronic contribution ($\kappa_e$) from $\kappa$. The electronic contribution was calculated via the Wiedemann-Franz relationship, $\kappa_e=LT/\rho$, within the limitations of a single-band approximation, from which the Lorenz number $L$ was obtained via common solutions to the Boltzmann transport equation,

$$L = \frac{k^2}{e^2}\frac{(1+\lambda)(3+\lambda)F_\lambda(\eta)F_{2+\lambda}(\eta) - (2+\lambda)^2F_{1+\lambda}(\eta)^2}{(1+\lambda)^2F_\lambda(\eta)^2}. \tag{9}$$

This expression assumes only one-electron-scattering mechanism is present (indicated by the value of $\lambda$) and the energy dependence of $\tau$ can be modeled by simple power law. Clearly the choice of scattering mechanism impacts $L$

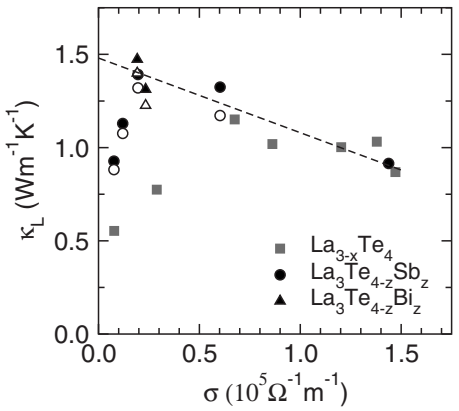


FIG. 11. The lattice thermal conductivity as a function of electrical conductivity at 573 K. For moderately large $\sigma$, $\kappa_L$ increases as $\sigma$ decreases (dashed line is a visual guide). This may be evidence for electron-phonon coupling, though the phonon group velocity increases as $\sigma$ decreases. At low $\sigma$, $\kappa_L$ is reduced by point-defect scattering, where the ability of vacancies to scatter phonons is highlighted. Filled symbols represent data obtained assuming acoustic phonon scattering limits $\mu$ and open symbols are for data obtained assuming ionized impurity scattering limits $\mu$.

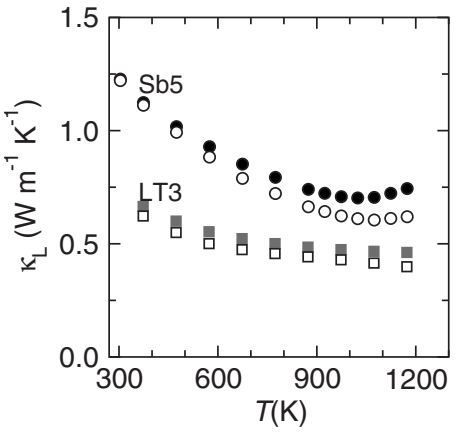


FIG. 12. The lattice thermal conductivity as a function of temperature reveals the temperature dependence expected for crystalline materials in Sb5, which is consistent with the reduced number of vacancies. The high concentration of vacancies in LT3 promotes a lower $\kappa_L$ with less temperature dependence. Open markers are obtained assuming ionized impurity scattering limits $\mu$, and the closed markers are obtained assuming acoustic phonon scattering limits $\mu$.

significantly. Acoustic phonon scattering ($\lambda=0$) appears to limit $\mu$ for low Sb content. For large Sb content, one could argue that ionized impurity scattering limits the carrier mobility at low or moderate $T$. Fortunately, at large Sb content, $\kappa_e$ is small regardless of the scattering assumption and thus the trends observed are not strongly dependent on the choice of scattering mechanism. To demonstrate the minor influence of $\lambda$ on $\kappa_L$, the values of $\kappa_L$ obtained from the limiting assumptions of $\lambda=0$ ($L \leq 2.44\times10^{-8}$ V$^2$ K$^{-2}$) and $\lambda=2$ ($L \geq 2.44\times10^{-8}$ V$^2$ K$^{-2}$) are compared in Figs. 11 and 12. Due to the small influence of $L$ for the low $\sigma$ compounds, the calculation of $L$ for the case of ionized impurity scattering has been simplified by assuming that $b$ defined by Eq. (8) is independent of carrier energy and thus $\lambda=2$ can be utilized in Eq. (9). As with theoretical $\mu_H$ curves, $\eta(T)$ is obtained from $\alpha(T)$.

The lattice thermal conductivity is plotted versus the electrical conductivity in Fig. 11, where data at 573 K are shown. The increase in $\kappa_L$ as $\sigma$ decreases may be linked to a decrease in electron-phonon interactions, the strength of which increase with increasing carrier mass.[20,21] According to Pippard,[21] when perfectly free electrons scatter acoustic phonons, the phonon mean free path $l_{e-p}$ scales with the free-electron concentration as

$$l_{e-p} \propto \frac{dv_s^2}{nm^* v_f}, \tag{10}$$

where $v_f$ and $v_s$ are the Fermi and mean sound velocities, respectively. This suggests that, if electron-phonon interactions limit $\kappa_L$, the value of $\kappa_L$ should decrease as carrier density $n$ increases. For the current system, a decrease in $n$ generally leads to a decrease in $m^*$ due to the multiband features shown in Fig. 6. We note Pippard's theory differs somewhat from that presented by Ziman for $l_{e-p}$, though the same $n$ dependence is observed in the $T\rightarrow\infty$ limit.[20] In general, these theories do not predict the scattering of phonons via electrons at moderate or high $T$, where the energetics are unfavorably, and thus this effect is expected to be small compared to Umklapp scattering (based on traditional theory).

Electron-phonon interactions are not the only explanation for the trends observed in Fig. 11. Calorimetry and inelastic neutron scattering have suggested the Debye temperature in $La_{3-x}Te_4$ increases by roughly 20% from $x=0$ to $\frac{1}{3}$.[9] This is believed to be due to the decrease in carrier concentration and the corresponding decrease in density of states at the Fermi level (reduction in ion-displacement screening), and thus this effect should be relatively similar in the $La_3Te_{4-z}Sb_z$ compounds where carrier concentration is reduced with Sb substitution. From kinetic theory, the lattice thermal conductivity is proportional to $v_s$ (which is proportional to the Debye temperature) and thus the 20% change in Debye temperature can explain much of the change in $\kappa_L$ shown in Fig. 11. We note that a ~4% reduction in $C_P$ is expected when $z$ increases from 0 to 1 due to a reduction in the electronic contribution (at 573 K), and less than a 1% increase is expected from the reduction in average atomic mass (for the Sb containing compounds). Therefore, we believe the changes in $\kappa_L$ are not the artifact of compositionally independent $C_P$.

In Fig. 11, it is observed that point-defect scattering significantly reduces $\kappa_L$ at low $\sigma$. This makes physical sense, as low $\sigma$ samples have large La vacancy content (for pure $La_{3-x}Te_4$) or high Sb concentrations. In $La_{3-x}Te_4$, a ~50% reduction in $\kappa_L$ occurs as $x$ increases from roughly 0 to 0.3, which demonstrates the strong scattering of phonons via vacancies. The reduction in $\kappa_L$ at large Sb content (filled circles) appears faster than expected for point-defect scattering by Sb ions alone (very little mass contrast to scattering phonons), and thus the data suggest an additional scattering source is present. Additional phonon scattering may arise due to local inhomogeneity or differences in microstructure that

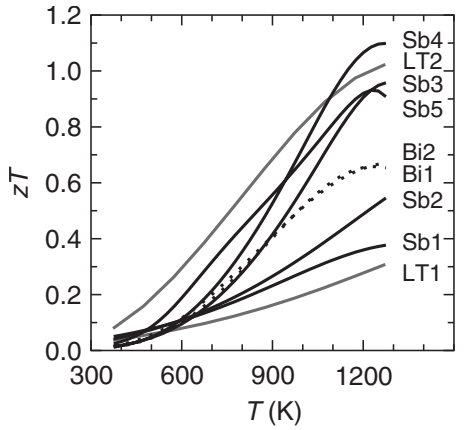


FIG. 13. Thermoelectric figure of merit versus temperature for representative pure $La_{3-x}Te_4$ (gray curves) samples are compared to those for Sb containing samples (solid black curves) and Bi containing samples (dotted curves) Above ~1000 K, the substitution of Sb for Te leads to minor improvement in $zT$, likely due to an increased carrier mobility though optimization of carrier density must also be considered.

are related to changes in the synthesis due at high Sb (Bi) concentration. Also, if $La_4Sb_3$ forms or anionic Sb sits on cationic La sites, additional phonon scattering would likely be observed. We note that the vacancy concentration inferred from Hall data and electron counting (assuming complete Sb substitution) suggests the vacancy concentration is fairly independent of Sb content, and thus vacancy formation is not utilized to explain the results at high Sb content.

The strong scattering of phonons via lanthanum vacancies leads to a nearly temperature independent $\kappa_L$ in sample LT3, see Fig. 12. In sample Sb5 (nominal $La_3Te_{3.2}Sb_{0.8}$), the reduced number of vacancies increases the effective crystallinity, thereby increasing $\kappa_L$ and promoting the usual decrease in $\kappa_L$ with increasing $T$ ($\sim T^{-1}$) expected for a crystalline material at high $T$. The temperature dependence of $\kappa_L$ for the samples containing Sb leads to low $\kappa_L$ at high $T$, thus allowing large thermoelectric performance to be achieved.

### C. Thermoelectric performance

The thermoelectric figure of merit is shown as a function of temperature in Fig. 13. For moderate temperatures, the large resistivity of high Sb content samples leads to low $zT$. At high $T$, however, the substitution of Sb for Te leads to modest improvements in $zT$ for sample Sb4. This appears to be due to an increased carrier mobility [as suggested by Fig. 9(b) for sample Sb5], though the effect of carrier density is difficult to isolate because only a small change in $zT$ is observed. The curves in Fig. 13 were generated from polynomial fits to the data presented above.

The reduced band gap associated with Sb or Bi substitution for Te causes $zT$ to reach a maximum value at lower temperatures than in pure $La_{3-x}Te_4$. This is readily observed in the data for the two Bi containing samples (dashed curves), which have a peak $zT$ near 1200 K. Reducing the band gap is one method associated with lowering the application temperature of a thermoelectric material. For this to be applied effectively, the effective mass of the majority carrier must be favorable coupled to the band gap, thus allowing an increase in $zT$ for a given temperature. In this case, it appears likely that the effective mass decreased with decreasing band gap, and the net effect on the high-temperature electronic properties was minor due to a balance in the changes in $|\alpha|$ and $\rho$ (for a given $n$).

## IV. CONCLUSION

The characterization and analysis of transport data in nominal $La_3Te_{4-z}Sb_z$ and $La_3Te_{4-z}Bi_z$ reveals the effect of band gap and phonon scattering by vacancies in the $La_{3-x}Te_4$ system. Seebeck coefficient measurements and density-functional calculations suggest the main change in electronic structure with Sb or Bi substitution is a reduction in the energy gap, though a decrease in electron effective mass is also inferred from transport data. Large Sb or Bi addition was found to promote activated electrical conduction at moderate $T$. This change in conduction is attributed to the onset of either ionized impurity scattering or hopping conduction. At large Sb content, the reduced point-defect scattering associated with La vacancies leads to a ~100% increase in $\kappa_L$, which highlights the ability of vacancies to scattering phonons in $La_{3-x}Te_4$. Despite a higher lattice thermal conductivity and electrical resistivity at moderate $T$, the $zT$ for nominal $La_3Te_{3.35}Sb_{0.65}$ is larger than that in the pure $La_{3-x}Te_4$ samples at high $T$. The increase in $zT$ is likely caused by an increase in carrier mobility, which is promoted by the reduction in lanthanum vacancy concentration and/or a decrease in electron effective mass upon Sb substitution. Thus, this work demonstrates a material whose large thermoelectric efficiency is relatively insensitive to the band gap.

## ACKNOWLEDGMENTS

We thank the DARPA Nano Materials Program for funding as well as the Jet Propulsion Laboratory for facilities and funding under contract with the National Aeronautics and Space Administration. E.F.-L. thanks the Norwegian Research Council and NOTUR project for support and facilities.

*may@caltech.edu

[1] A. F. May, D. J. Singh, and G. J. Snyder, Phys. Rev. B **79**, 153101 (2009).

[2] L. Danielson, M. Alexander, C. Vining, R. Lockwood, and C. Wood, Proceedings Seventh International Conference on Thermoelectric Energy Conversion, 1988 (unpublished), p. 71.

[3] C. Vining, C. Wood, J. Parker, A. Zoltan, L. Danielson, and M. Alexander, Proceedings Seventh International Conference on Thermoelectric Energy Conversion, 1988 (unpublished), p. 9.
[4] A. F. May, J.-P. Fleurial, and G. J. Snyder, Phys. Rev. B **78**, 125205 (2008).
[5] S. R. Brown, S. M. Kauzlarich, F. Gascoin, and G. J. Snyder, Chem. Mater. **18**, 1873 (2006).
[6] E. S. Toberer and G. J. Snyder, Nature Mater. **7**, 105 (2008).
[7] M. Cutler and N. F. Mott, Phys. Rev. **181**, 1336 (1969).
[8] C. Wood, D. Zoltan, and G. Stapfer, Rev. Sci. Instrum. **56**, 719 (1985).
[9] O. Delaire, A. F. May, M. A. McGuire, W. D. Porter, D. L. Abernathy, and G. J. Snyder, Phys. Rev. B **80**, 184302 (2009).
[10] G. Kresse and J. Hafner, Phys. Rev. B **48**, 13115 (1993).
[11] G. Kresse and J. Furthmüller, Phys. Rev. B **54**, 11169 (1996).
[12] J. P. Perdew, K. Burke, and M. Ernzerhof, Phys. Rev. Lett. **77**, 3865 (1996).
[13] J. Flahaut, M. Guittard, M. Patrie, M. Pardo, S. Golabi, and L. Domange, Acta Crystallogr. **19**, 14 (1965).
[14] P. Pulay, Chem. Phys. Lett. **73**, 393 (1980).
[15] P. E. Blöchl, O. Jepsen, and O. K. Andersen, Phys. Rev. B **49**, 16223 (1994).
[16] V. I. Fistul, *Heavily Doped Semiconductors* (Plenum Press, New York, 1969).
[17] H. J. Goldsmid and J. W. Sharp, J. Electron. Mater. **28**, 869 (1999).
[18] J. H. Shim, K. Kim, B. I. Min, and J. S. Kang, Physica B **328**, 148 (2003).
[19] D. Chattopadhyay and H. J. Queisser, Rev. Mod. Phys. **53**, 745 (1981).
[20] J. M. Ziman, Philos. Mag. **1**, 191 (1956).
[21] A. B. Pippard, Philos. Mag. **46**, 1104 (1955).